Benchmarking the spiky and mixed-kernel approaches

Here we benchmark our mixed-kernel approach against the 1D Shock Tube problem – a well-known benchmark in the SPH community (eg. Sod, 1978; Monaghan and Gingold, 1983, Hernquist and Katz, 1989) for which an iterative analytical solution exists. We adopt the following initial conditions:

$x < 0,\ \rho = 1,\ v = 0,\ e = 2.5,\ P=1,\ \Delta x = 0.001875;$
$x \geq 0,\ \rho = 0.25,\ v = 0,\ e = 1.795,\ P=0.1795,\ \Delta x = 0.0075;$

Here ρ is the density, v the particle velocity, e the internal energy, P the pressure, and Δx the initial particle spacing. 400 particles are used, and the mass of each particle is m=0.001875. 320 particles are distributed along the high density zone ($-0.6 < x < 0.0$), and 80 in the low density zone ($0 \leq x < 0.6$). We use an ideal gas equation of state of the form:

$$P = (\gamma - 1)\,\rho e \qquad \text{(Equation S.1)}$$

Where γ is 1.4. The timestep is 0.05, and we have also used an artificial viscosity of the form of Equation S.12, where $\alpha_{\prod}$ and $\beta_{\prod}$ are 1 and 2, respectively. We have not included any treatment of the boundaries, nor have included improvements to handle the shock front (eg. CSPH, or DSPH or Liu and Liu, 2004). We present the results for Gaussian, cubic splines, mixed kernels, and spiky kernels.

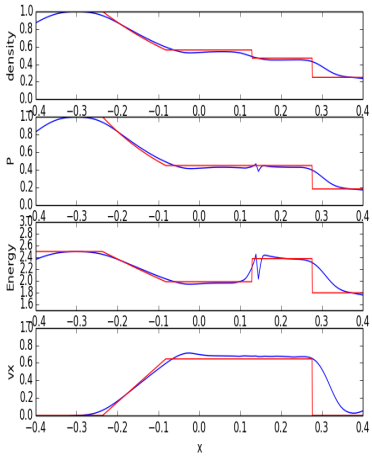

Figure S.1. Analytical (red) and SPH (blue) solutions for the Sod (1978) shock tube problem, for a Gaussian kernel, at t=0.2s. The shock is around x=0.3, and the rarefaction between x=-0.3 and 0. The contact discontinuity is between x=0.1 and 0.2.

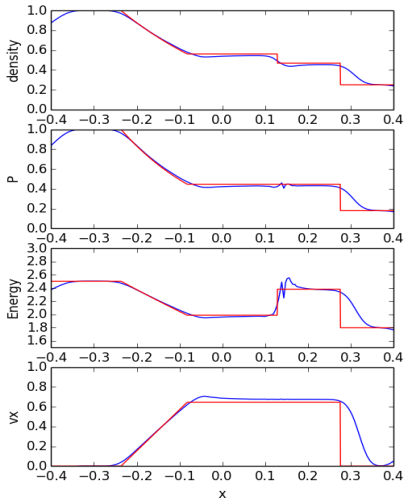

Figure S.2. Analytical (red) and SPH (blue) solutions for the Sod (1978) shock tube problem, for a cubic spline kernel, at t=0.2s.

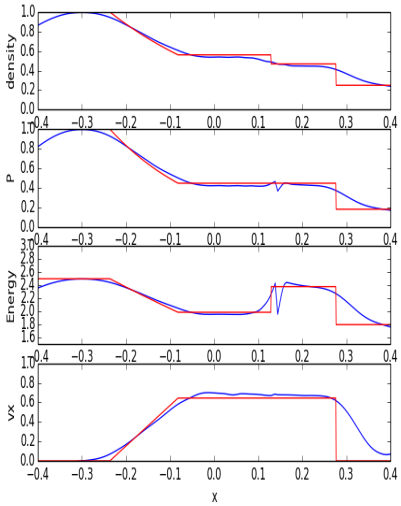

Figure S.3. Analytical (red) and SPH (blue) solutions for the Sod (1978) shock tube problem, for a mixed spline/ quartic kernel, at t=0.2s.

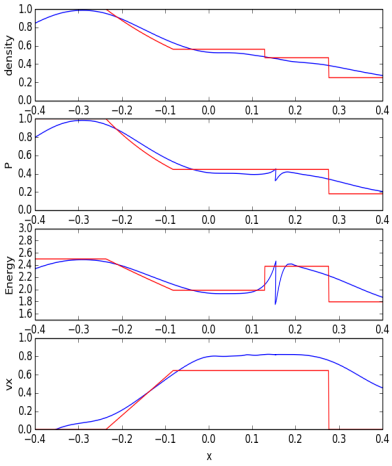

Figure S.4. Analytical (red) and SPH (blue) solutions for the Sod (1978) shock tube problem, for a 1D spiky kernel, at t=0.2s.

While the problem has not been optimized for resolving shock fronts, the results are comparable for each of these four kernel approaches, and for the analytical solution. Primary differences include the spiky kernel smearing out velocities at the shock front, due to the high pressures between closely spaced particles – a behavior that is desirable in planetary interiors to avoid particle clustering at high pressures.

Benchmarking the viscosity formulation and sinking problem

The following benchmark is adopted from Liu and Liu et al. (2003), for a shear-driven cavity flow. The full simulation is described in section 4.3 of that book. We adopt the same physical set-up. The cavity itself is defined by 3 edges of zero velocity, and a top edge which moves with a constant speed of 10^{-3} ms^{-1}, to the right. The dimensions of the box are l=10^{-3} m, the viscosity is 10^{-3} Pa.s, and the density is 1000kg/m^3, giving a Reynolds number of 1 for the problem.

The initial configuration is a grid of 40x40 real particles, with 320 (81 per side) virtual particles defining the edges. The virtual particle's velocity and position are not updated. The velocities of these particles define the boundary conditions of the problem. In addition to standard SPH interactions, the virtual boundary particles interact via a Lennard-Jones style boundary force, defined by:

$$PB_{ij} = \begin{cases} D\left[\left(\frac{r_0}{r_{ij}}\right)^{n_1} - \left(\frac{r_0}{r_{ij}}\right)^{n_2}\right]\frac{x_{ij}}{r_{ij}^2} & \left(\frac{r_0}{r_{ij}}\right) \leq 1 \\ 0 & \left(\frac{r_0}{r_{ij}}\right) \leq 1 \end{cases}$$

(Equation S.2)

Here D is 0.01, n_1 is 12, and n_2 is 4. The distance between particles i and j is r_{ij}, and r_0 is taken to be the 2.0e-5. We use a Wendland style kernel for this example (Wendland, 1995), of the form (in 2D):

$$W(r,h) = \frac{7}{4\pi h^2}\left(1 - \frac{q}{2}\right)^4 (2q+1) \quad 0 \leq q \leq 2$$

(Equation S.3)

Not q is r/h. Kernel smoothing width h is 2.5e-5. We have also included an XSPH correction to prevent interpenetration of particle flow:

$$\frac{dx_i}{dt} = v_i - \varepsilon \sum_j \frac{m_j}{\rho_j} v_{ij} W_{ij}$$

(Equation S.4)

Here we take ε to be 0.3. We use a Morris (1997) equation of state as per Liu and Liu (2003):

$$p = c^2\rho$$

(Equation S.5)

Here p is pressure, ρ is density, and c is an 'artificial' sound speed, taken to be 0.01m/s, based on the maximum system velocities. We use a constant timestep of 5e-5 as per Liu and Liu (2003), and run the simulation until steady-state is reached. Our initial configuration, and steady-state flow, are shown in Figure S.5, and agree well with Liu and Liu's results.

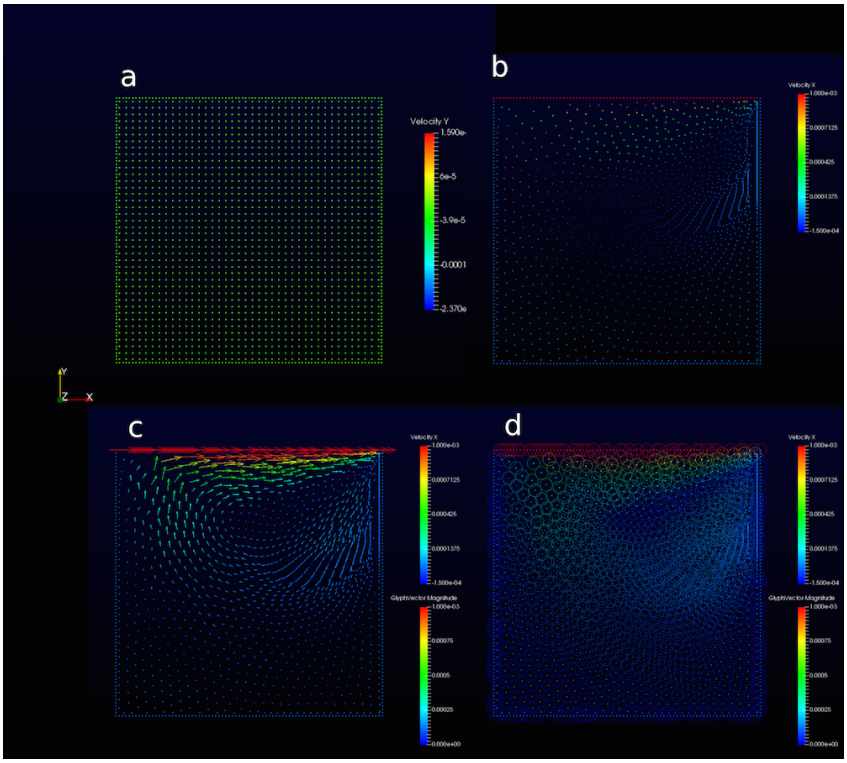

Figure S.5. Initial particle configuration (a) and steady-state particle configuration (b) for the shear-cavity problem described in the text. C) and d) show the final velocity field, and particle kernel smoothing widths, respectively.

Finally, we modify this benchmark to describe the sinking of a dense mass within a viscous liquid. We use the same set-up as previously, but set all boundary conditions to zero velocity, and the artificial sound speed to 5m/s as system velocities are greater. The dense blob is differentiated by a different rest density (1500kg/m^3, as opposed to 1000kg/m^3 for the surrounding fluid), which makes the particles draw closer together, increasing the local density of the fluid. We have also included a gravitational force for the negatively buoyant particles, of the order $-9.81\Delta\rho$, where $\Delta\rho$ represents the local density difference between the dense fluid and ambient fluid. Previous work suggests that the velocity of a downgoing conduit should scale as

$$v \sim (1/\mu)^{0.5}$$

Where v is the velocity in the conduit, and μ the viscosity (note other scalings exist, for developing drip, for instance, but are qualitatively similar). The following plots show the material distribution, and y component of velocity, for a typical simulation.

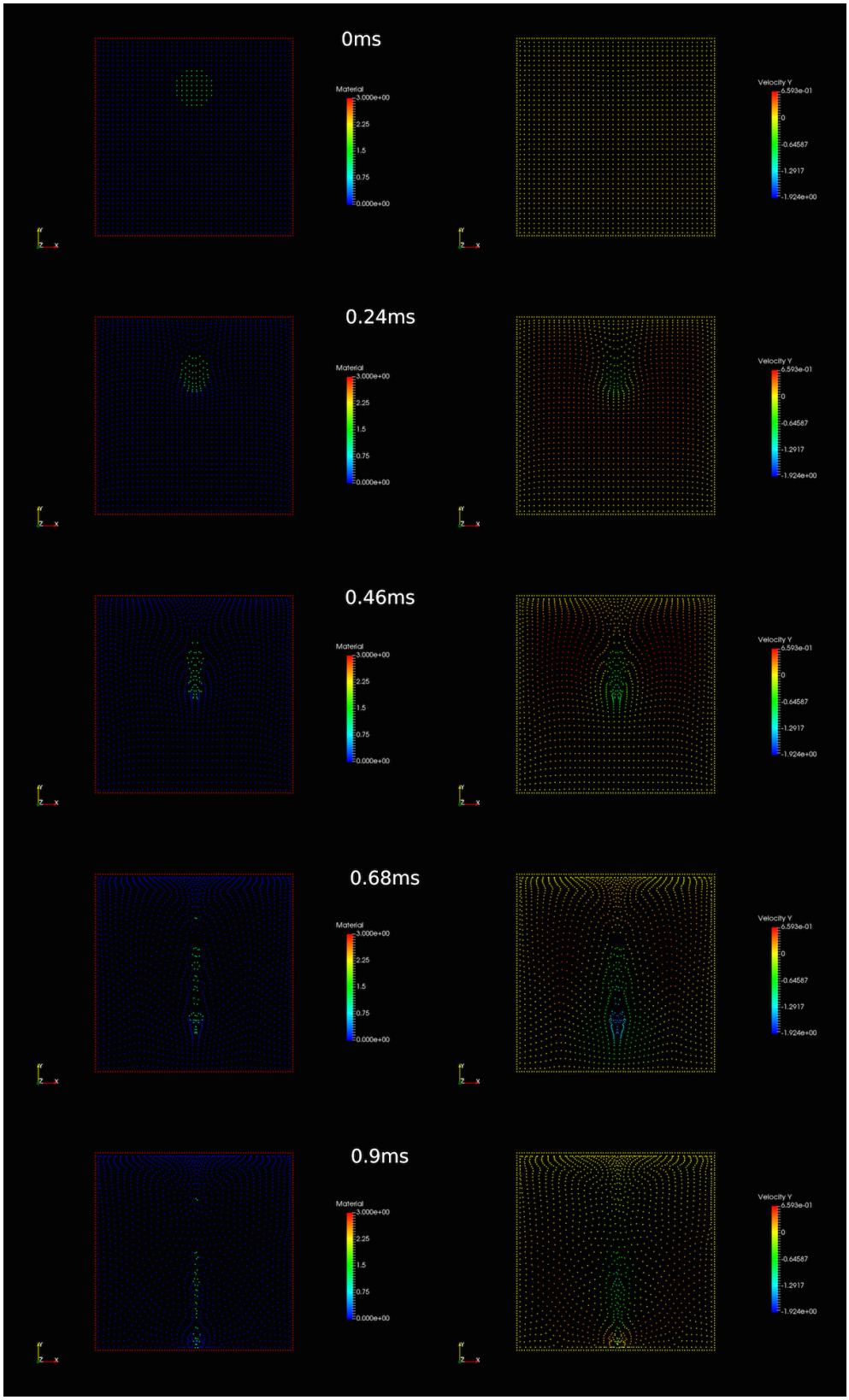

Figure S.6. Evolution of a dense viscous blob in a viscous fluid. Left: material distribution. Dense material shown as green, blue shows background viscous material, and red represents boundary particles. Viscosity of background material and blob are the same (here 5e3Pa.s). Right: particle shading shows vertical velocity magnitude, showing rapid downwelling associated with the dense material, which then pools on the bottom, and counter-flow of the lighter background liquid.

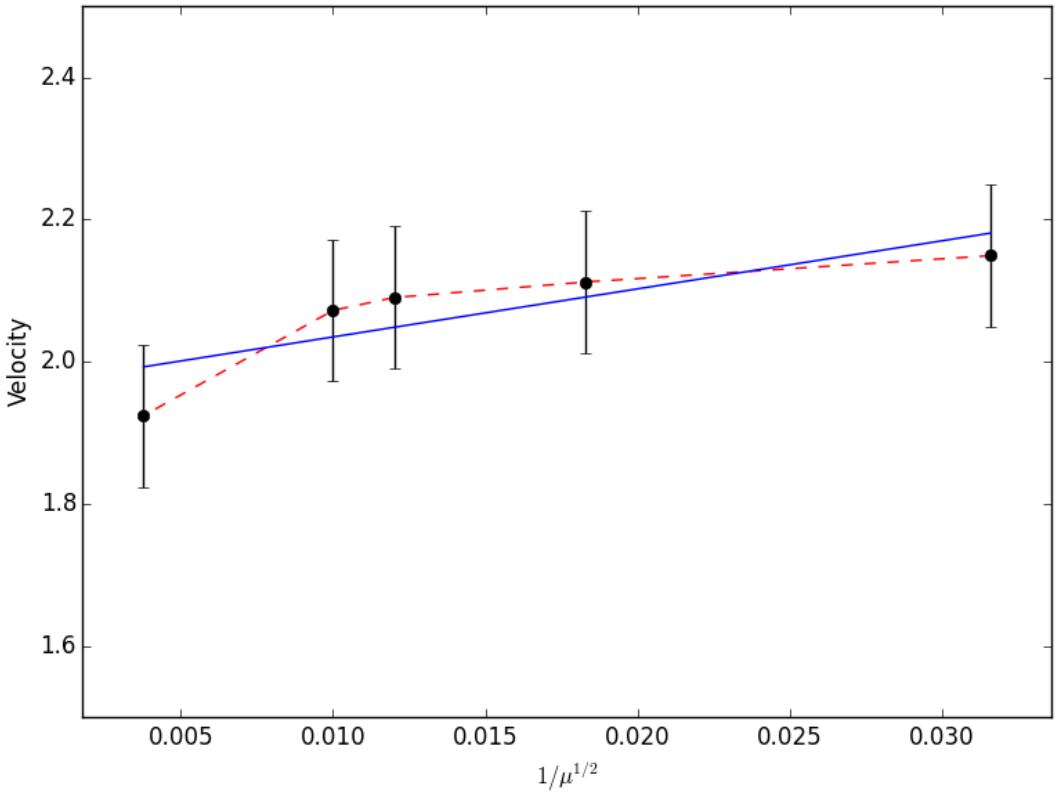

Figure S.7. Plot of maximum system velocity vs $(1/\mu)^{0.5}$, for the simulation configuration shown in Figure S.6. Note blob and background viscosities are the same in all examples. The viscous blob sinks faster for lower viscosities, and the relationship shows a linear $(1/\mu)^{0.5}$ trend, though boundary conditions do have an effect due to limited domain size. Blue represents the line of best fit, velocity error bars represent standard deviation in maximum velocities.

Additional references:

Morris J. P., Fox P. J. and Zhu Y. (1997), Modeling low Reynolds number incompressible flows using SPH, Journal of Computational Physics, 136:214-226.
Wendland, H. (2006). Computational aspects of radial basis function approximation. *Studies in Computational Mathematics*, *12*, 231-256.